Electronic Supplementary Material (ESI) for CrystEngComm.

Supporting Information

Charge Control the Formation of Two Neutral/Cationic Metal–Organic Frameworks Based on Neutral/Cationic Triangular Clusters and Isonicotinic Acid: Structure, Gas Adsorption and Magnetism

Lei Zhou, Baolei Zhou, Zheng Cui, Bowen Qin, Xiaoying Zhang*, Wenliang Li* and Jingping Zhang*

Advanced Energy Materials Research Center, Faculty of Chemistry, Northeast Normal University, Changchun 130024, P. R. China

Corresponding Author

* jpzhang@nenu.edu.cn

* zhangxy218@nenu.edu.cn

* liwl926@nenu.edu.cn

Table S1. The crystallographic data for complexes **Mn-Ac** and **Co-DMA**.

Compound	**Mn-Ac**	**Co-DMA**
empirical formula	$C_{26}H_{24}N_4O_{13}Mn_3$	$C_{72}H_{104}N_{14}O_{40}Cl_2Co_6$
M_r	765.30	2230.07
T (K)	293(2)	293(2)
Crystal system	orthorhombic	orthorhombic
Space group	*P*nnm	*P*nma
a (Å)	12.402	19.582
b (Å)	14.734	20.1291
c (Å)	20.85	12.0113
α (deg)	90	90
β (deg)	90	90
γ (deg)	90	90
V (Å^3)	3809.943	4734.5(4)
Z	4	2
ρ_{calcd}/g cm^{-3}	1.303	1.366
GOF	1.125	1.061
R_1 [$I > 2\sigma(I)$]	0.0437	0.0786
wR_2 [$I > 2\sigma(I)$]	0.1285	0.2356

$R_1 = \sum(||F_0| - |F_c||)/\sum|F_0|$. $wR_2 = [\sum w(|F_0|^2 - |F_c|^2)^2/\sum w(F_0^2)^2]^{1/2}$.

Table S2. Selected bond lengths (Å) and angles (°) for **Mn-Ac**.

Bond lengths [Å]			
Mn(1)-O(2)#1	2.150(2)	Mn(2)-O(4)	2.137(2)
Mn(1)-O(2)	2.150(2)	Mn(2)-O(3)	2.155(2)
Mn(1)-O(1)	2.163(3)	Mn(2)-O(6)	2.160(2)
Mn(1)-O(7)	2.211(3)	Mn(2)-O(1)	2.1608(16)
Mn(1)-N(2)#2	2.310(4)	Mn(2)-O(5)	2.244(2)
Mn(1)-N(3)#3	2.315(4)	Mn(2)-N(1)#4	2.327(3)
Angles [deg]			
O(2)#1-Mn(1)-O(2)	164.65(13)	O(4)-Mn(2)-O(3)	96.46(12)
O(2)#1-Mn(1)-O(1)	96.65(7)	O(4)-Mn(2)-O(6)	90.39(12)
O(2)-Mn(1)-O(1)	96.65(7)	O(3)-Mn(2)-O(6)	161.91(10)
O(2)#1-Mn(1)-O(7)	86.73(7)	O(4)-Mn(2)-O(1)	90.34(11)
O(2)-Mn(1)-O(7)	86.73(7)	O(3)-Mn(2)-O(1)	97.34(9)
O(1)-Mn(1)-O(7)	85.50(12)	O(6)-Mn(2)-O(1)	99.35(9)
O(2)#1-Mn(1)-N(2)#2	92.98(7)	O(4)-Mn(2)-O(5)	172.18(10)

O(2)-Mn(1)-N(2)#2	92.98(7)	O(3)-Mn(2)-O(5)	89.87(11)
O(1)-Mn(1)-N(2)#2	96.91(13)	O(6)-Mn(2)-O(5)	84.90(11)
O(7)-Mn(1)-N(2)#2	177.59(14)	O(1)-Mn(2)-O(5)	84.28(11)
O(2)#1-Mn(1)-N(3)#3	82.90(6)	O(4)-Mn(2)-N(1)#4	88.31(10)
O(2)-Mn(1)-N(3)#3	82.90(6)	O(3)-Mn(2)-N(1)#4	81.35(9)
O(1)-Mn(1)-N(3)#3	172.42(13)	O(6)-Mn(2)-N(1)#4	82.14(9)
O(7)-Mn(1)-N(3)#3	86.92(14)	O(1)-Mn(2)-N(1)#4	178.00(11)
N(2)#2-Mn(1)-N(3)#3	90.67(14)	O(5)-Mn(2)-N(1)#4	97.21(10)

Symmetry Code: #1 x,y,-z; #2 -x,-y,-z; #3 x-1,y,z; #4 x+1/2,-y+1/2,-z+1/2.

Table S3. BVS calculations for the Mn ions in complex **Mn-Ac**.

Atom	**Mn^{II}**	**Mn^{III}**	**Mn^{IV}**	**Mn^{VII}**
Mn1	2.04	1.93	1.90	2.04
Mn2	2.08	1.94	1.91	2.08

Table S4. Selected bond lengths (Å) and angles (°) for **Co-DMA**.

Bond lengths [Å]			
Co(1)-O(2)	2.045(4)	Co(2)-O(1)	2.079(5)
Co(1)-O(4)	2.053(7)	Co(2)-O(3)#1	2.086(4)
Co(1)-O(6)	2.074(5)	Co(2)-O(3)	2.086(4)
Co(1)-O(5)	2.099(4)	Co(2)-N(3)	2.157(7)
Co(1)-O(1)	2.100(3)	Co(2)-O(8)	2.178(7)
Co(1)-O(7)	2.127(6)	Co(2)-N(2)	2.187(6)
Co(1)-N(1)	2.188(5)		
Angles [deg]			
O(2)-Co(1)-O(4)	161.3(3)	O(5)-Co(1)-N(1)	84.03(18)
O(2)-Co(1)-O(6)	86.9(3)	O(1)-Co(1)-N(1)	175.7(2)
O(4)-Co(1)-O(6)	81.7(3)	O(7)-Co(1)-N(1)	90.4(2)
O(2)-Co(1)-O(5)	164.1(2)	O(1)-Co(2)-O(3)#1	96.69(11)
O(4)-Co(1)-O(5)	22.8(2)	O(1)-Co(2)-O(3)	96.69(11)
O(6)-Co(1)-O(5)	104.3(2)	O(3)#1-Co(2)-O(3)	166.5(2)
O(2)-Co(1)-O(1)	96.66(17)	O(1)-Co(2)-N(3)	92.7(2)
O(4)-Co(1)-O(1)	98.9(2)	O(3)#1-Co(2)-N(3)	90.60(13)
O(6)-Co(1)-O(1)	93.8(2)	O(3)-Co(2)-N(3)	90.60(13)

O(5)-Co(1)-O(1)	93.85(18)	O(1)-Co(2)-O(8)	86.8(2)
O(2)-Co(1)-O(7)	93.8(3)	O(3)#1-Co(2)-O(8)	89.46(13)
O(4)-Co(1)-O(7)	97.8(3)	O(3)-Co(2)-O(8)	89.46(13)
O(6)-Co(1)-O(7)	179.1(2)	N(3)-Co(2)-O(8)	179.5(2)
O(5)-Co(1)-O(7)	75.2(2)	O(1)-Co(2)-N(2)	176.4(2)
O(1)-Co(1)-O(7)	85.4(2)	O(3)#1-Co(2)-N(2)	83.26(11)
O(2)-Co(1)-N(1)	84.67(17)	O(3)-Co(2)-N(2)	83.26(11)
O(4)-Co(1)-N(1)	80.6(2)	N(3)-Co(2)-N(2)	90.9(3)
O(6)-Co(1)-N(1)	90.3(2)	O(8)-Co(2)-N(2)	89.6(3)

Symmetry Code: #1 x,-y+1/2,z.

Table S5. BVS calculations for the Co ions in complex **Co-DMA**.

Atom	Co^{II}	Co^{III}
Co1	2.14	2.18
Co2	2.09	2.12

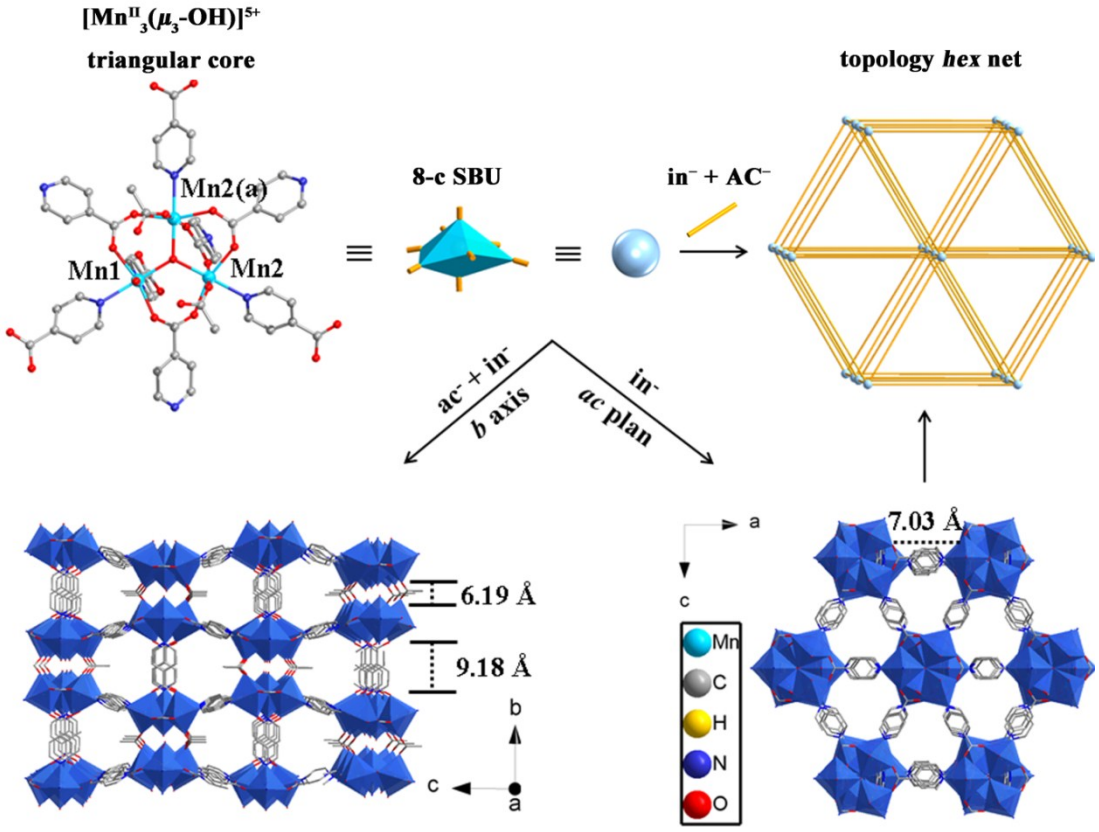

Fig. S1 View of the coordination environment of [Mn_3-CH_3COO^-] triangular core. The [Mn_3-CH_3COO^-] units, acting as 8-connected nodes, are interlinked by a double-CH_3COO^- and a double-in^- linkers above and below the *ac* plane, respectively and six in^- linkers in *ac* plane to form a 3D open framework **Mn-Ac** with 8-connected *hex* topology. H atoms are omitted for clarity. Symmetry Code: a x,y,-z.

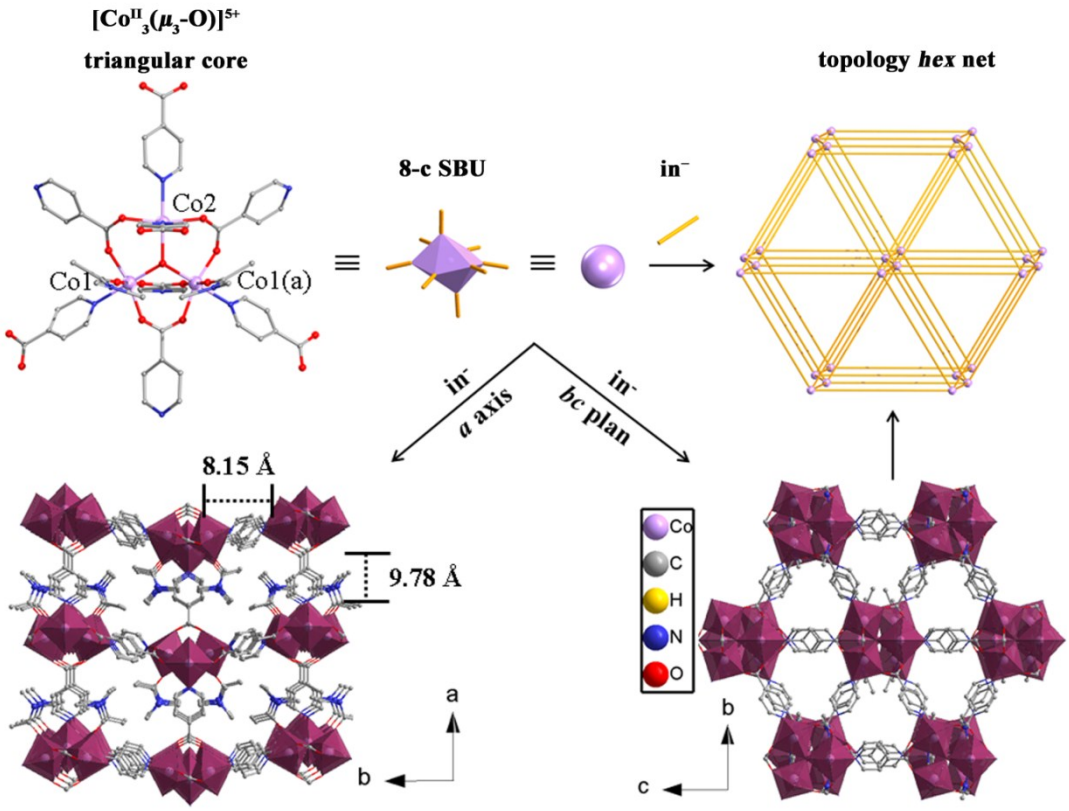

Fig. S2 View of the coordination environment of [Co_3-DMA] triangular core. The [Co_3-DMA] units, acting as 8-connected nodes, are interlinked by eight in$^-$ linkers to form a 3D open framework **Co-DMA** with 8-connected *hex* topology. H atoms are omitted for clarity. Symmetry Code: a x,0.5-y,z.

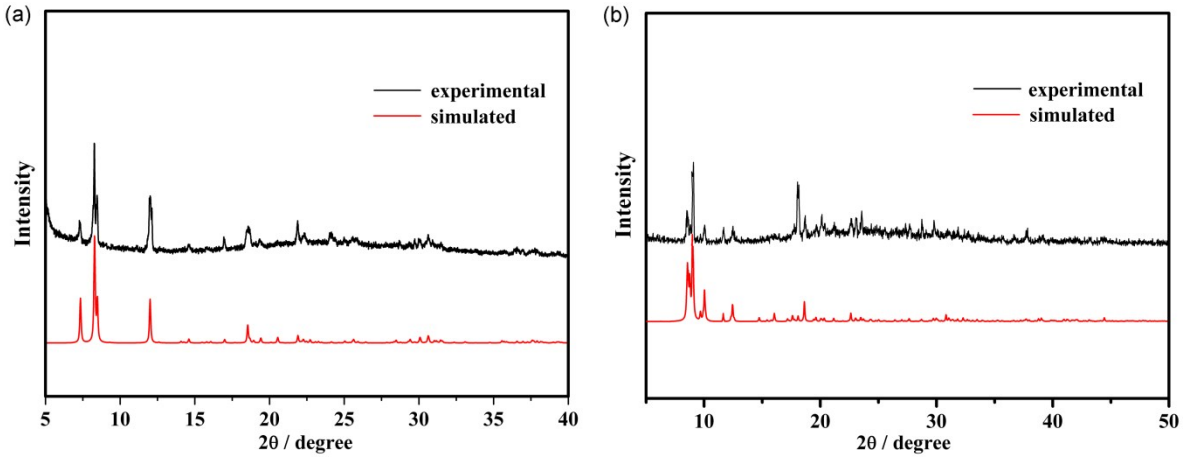

Fig. S3 The PXRD patterns of **Mn-Ac** (**a**) and **Co-DMA** (**b**).

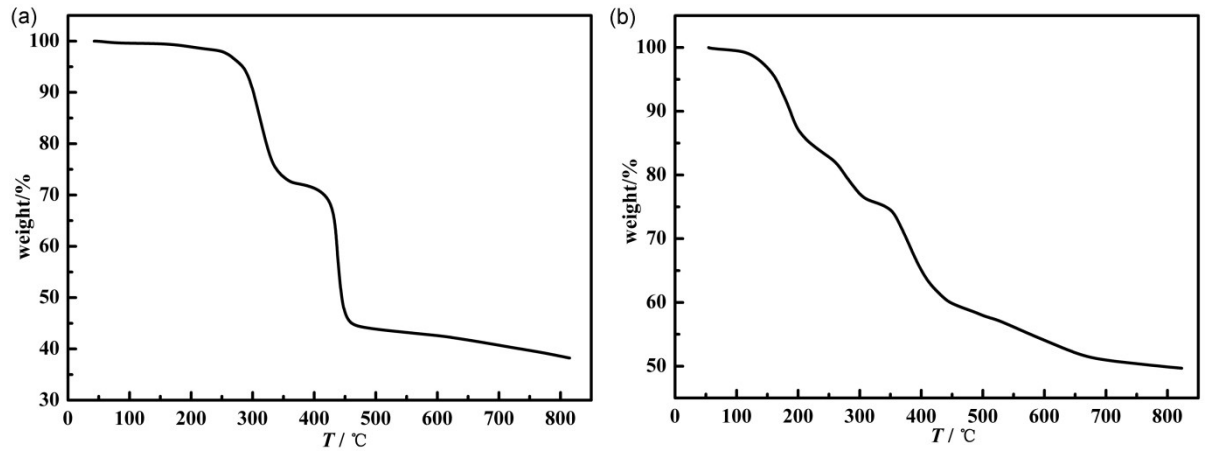

Fig. S4 The TGA curves of **Mn-Ac** (**a**) and **Co-DMA** (**b**).

Sorption properties

The as-synthesized **Mn-Ac** and **Co-DMA** (~100 mg) samples were washed three times with EtOH/MeCN and DMA, respectively. After that, they were placed in 20 ml vial without sealed caps and were heated under vacuum at 85°C for 24 h. Before the adsorption measurements, the samples were dried through the "degas" function of the adsorption instrument for 12 h at 100°C.

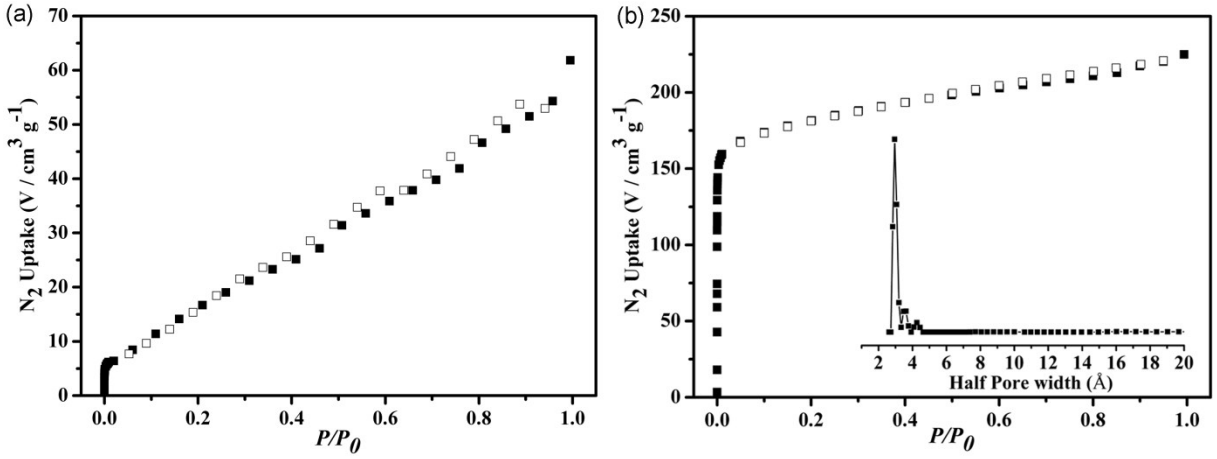

Fig. S5 (a) N_2-adsorption isotherms at 77 K for **Mn-Ac** (a) and **Co-DMA** (b). Filled and open symbols represent adsorption and desorption branches respectively. (Inset) Pore size distribution analyzed by DFT methods.

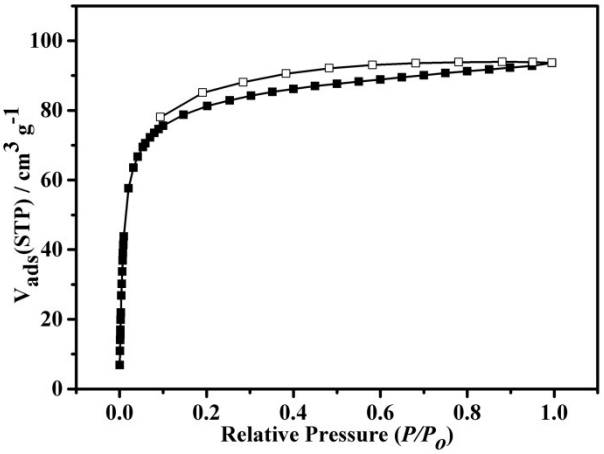

Fig. S6 CO_2 sorption isotherm of **Mn-Ac** at 195 K.

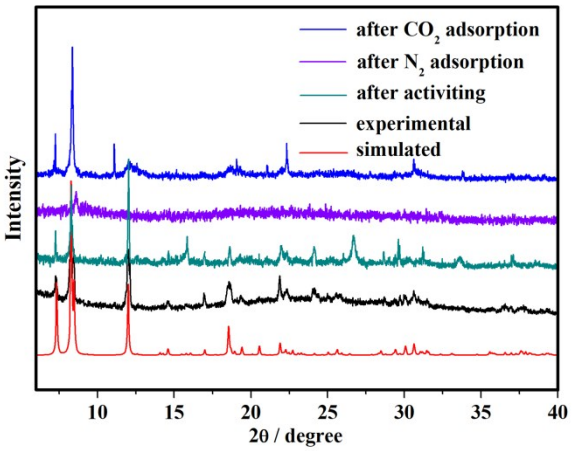

Fig. S7 (a) The PXRD patterns of **Mn-Ac** after an activation process and samples are measured with CO_2 and N_2.

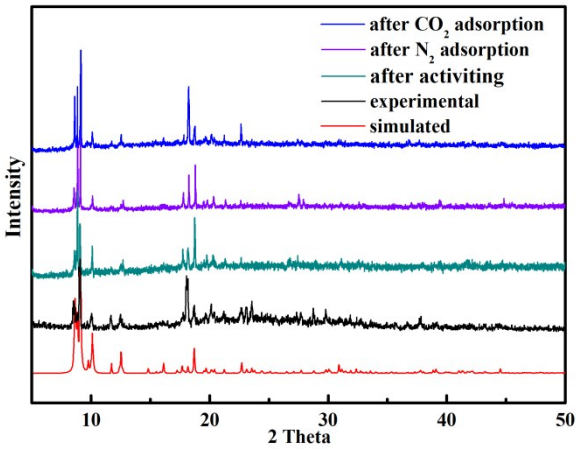

Fig. S8 (a) The PXRD patterns of **Co-DMA** after an activation process and after samples are measured with CO_2 and N_2.

CO_2/CH_4 and CO_2/N_2 Selectivity Prediction via Henry's law

The experimental isotherm data for pure CO_2, CH_4 and N_2 were fitted using a Single-site Langmuir model:

$$V_{ads}^{\ i} = \frac{V_{1i}K_{1i}P}{1 + K_1P}$$

Where V_{ads} is the total amount adsorbed in $cm^3\ g^{-1}$, P is the applied pressure in atm, V_i is the saturation capacity in $cm^3\ g^{-1}$, and K_i is the Langmuir affinity constant expressed in atm^{-1}. The fitting of the isotherm models was achieved by calculating the K_i and V_i parameters.

Selectivity at low coverage was calculated using the results of the single-site Langmuir fits of the experimental isotherms, by determining the Henry constants for each gas (Table S7 and S7) based on the equation:

$$H_i = \sum K_i V_i$$

The selectivity at zero pressure is then calculated with the relation:

$$S_{1,2} = \frac{H_1}{H_2}$$

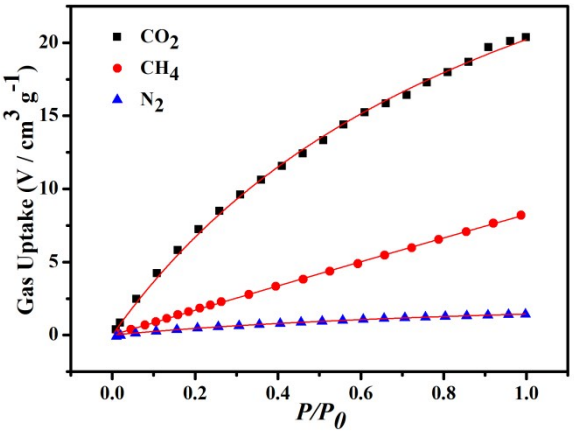

Fig. S9 Adsorption isotherms of CO_2, CH_4 and N_2 recorded at 298 K for compound **Mn-Ac**. Solid lines represent fitting curves using a single-site Langmuir model.

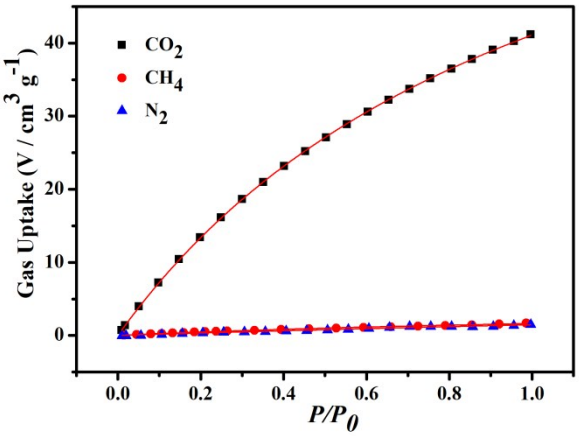

Fig. S10 Adsorption isotherms of CO_2, CH_4 and N_2 recorded at 298 K for compound **Co-DMA**. Solid lines represent fitting curves using a single-site Langmuir model.

Table S6. Summary of the gas uptake at 298 K under 1 atm for the two MOFs **Mn-Ac** and **Co-DMA**.

	CO_2 $cm^3\ g^{-1}$	CH_4 $cm^3\ g^{-1}$	N_2 $cm^3\ g^{-1}$
Mn-Ac	20.37	8.14	1.43
Co-DMA	41.18	1.44	1.45

Table S7. Fit parameters for the CO_2 and CH_4 isotherms of compound **Mn-Ac** at 298 K and selectivity.

Mn-Ac	**CO_2**	**CH_4**	**N_2**	**CO_2/CH_4 selectivity[c]**	**CO_2/N_2 selectivity[c]**
V_i[a]	40.90	259.39	3.12	4.7	15.1
K_i[b]	0.978	0.03	0.85		

[a] Saturation uptakes and [b] affinity constants estimated from a single Langmuir site model; [c] Selectivity estimated from the ratio of the Henry constant (= ratio of the initial slopes) at 298 K.

Table S8. Fit parameters for the CO_2 and CH_4 isotherms of compound **Co-DMA** at 298 K and selectivity.

Co-DMA	**CO_2**	**CH_4**	**N_2**	**CO_2/CH_4 selectivity[c]**	**CO_2/N_2 selectivity[c]**
V_i[a]	85.39	4.37	11.64	30.8	48.7
K_i[b]	0.929	0.589	0.14		

[a] Saturation uptakes and [b] affinity constants estimated from a single Langmuir site model; [c] Selectivity estimated from the ratio of the Henry constant (= ratio of the initial slopes) at 298 K.

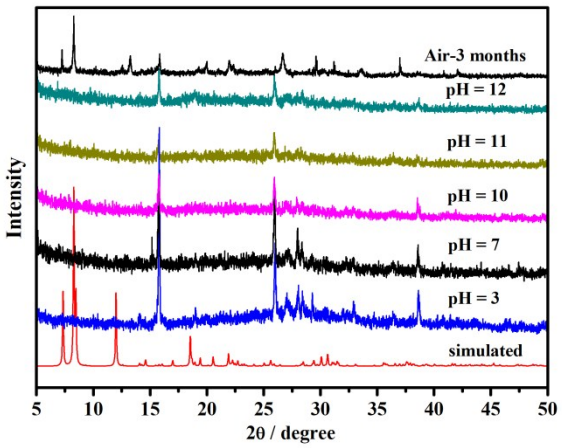

Fig. S11 The PXRD patterns of **Mn-Ac** after samples are soaked in aqueous, acidic or basic solutions for 1 h and under air condition at room temperature.

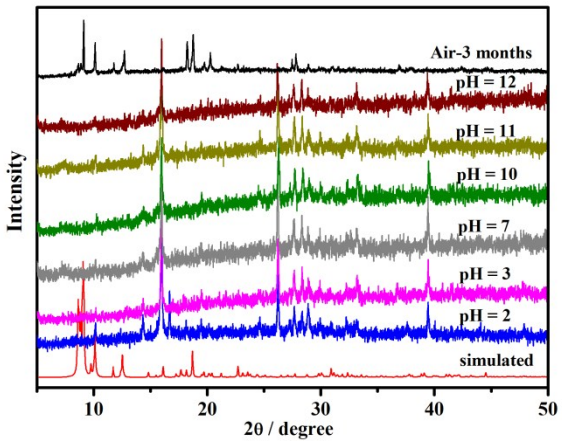

Fig. S12 The PXRD patterns of **Co-DMA** after samples are soaked in aqueous, acidic or basic solutions for 1 h and under air condition at room temperature.

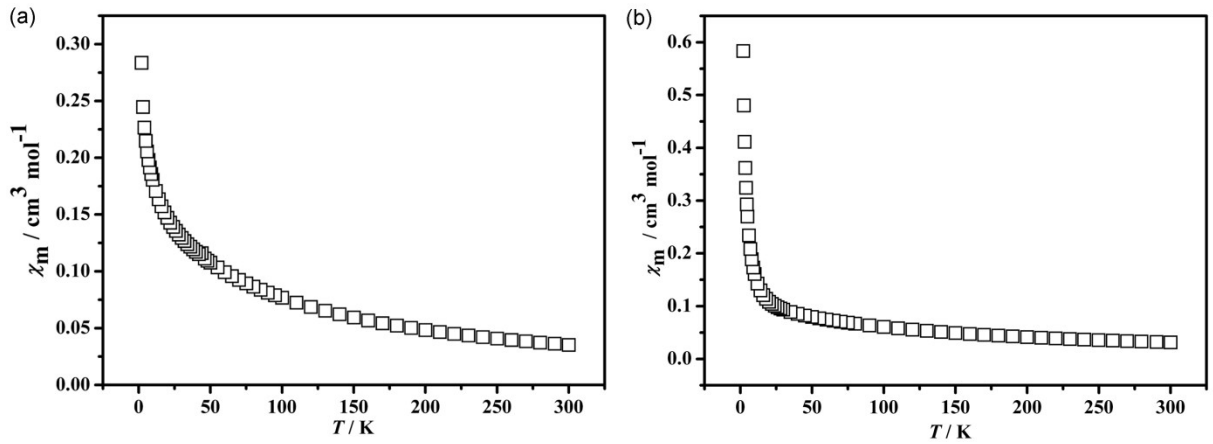

Fig. S13 The temperature dependence of χ_m curves for **Mn-Ac** (**a**) and **Co-DMA** (**b**) under a static field of 1000 Oe.

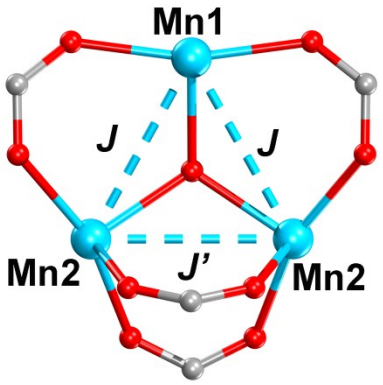

Fig. S14 Geometrical model of complex **Mn-Ac**.

Equation.

Theoretical expression for χ_m derived from van Vleck equation with the simplified Heisenberg Hamiltonian. The equation (1) is used for the analysis of complexe **Mn-Ac**.

$\chi_m T$ = 0.125×p1×p1×[52.5×exp(8.75×p2/x)+15×exp(1.75×p2/x+2×p3/x)+52.5×exp(6.75×p2/x+2×p3/x)+126×exp(13.75×p2/x+2×p3/x)+1.5×exp(-5.25×p2/x+6×p3/x)+15×exp(-2.25×p2/x+6×p3/x)+52.5×exp(2.75×p2/x+6×p3/x)+126×exp(9.75×p2/x+6×p3/x)+247.5×exp(18.75×p2/x+6×p3/x)+1.5×exp(-11.25×p2/x+12×p3/x)+15×exp(-8.25×p2/x+12×p3/x)+52.5×exp(-3.25×p2/x+12×p3/x)+126×exp(3.75×p2/x+12×p3/x)+247.5×exp(12.75×p2/x+12×p3/x)+429×exp(23.75×p2/x+12×p3/x)+15×exp(-16.25×p2/x+20×p3/x)+52.5×exp(-11.25×p2/x+20×p3/x)+126×exp(-4.25×p2/x+20×p3/x)+247.5×exp(4.75×p2/x+20×p3/x)+429×exp(15.75×p2/x+20×p3/x)+682.5×exp(28.75×p2/x+20×p3/x)+52.5×exp(-21.25×p2/x+30×p3/x)+126×exp(-14.25×p2/x+30×p3/x)+247.5×exp(-5.25×p2/x+30×p3/x)+429×exp(5.75×p2/x+30×p3/x)+682.5×exp(18.75×p2/x+30×p3/x)+1020×exp(33.75×p2/x+30×p3/x)]/[6×exp(8.75×p2/x)+4×exp(1.75×p2/x+2×p3/x)+6×exp(6.75×p2/x+2×p3/x)+8×exp(13.75×p2/x+2×p3/x)+2×exp(-5.25×p2/x+6×p3/x)+4×exp(-2.25×p2/x+6×p3/x)+6×exp(2.75×p2/x+6×p3/x)+8×exp(9.75×p2/x+6×p3/x)+10×exp(18.75×p2/x+6×p3/x)+2×exp(-11.25×p2/x+12×p3/x)+4×exp(-8.25×p2/x+12×p3/x)+6×exp(-3.25×p2/x+12×p3/x)+8×exp(3.75×p2/x+12×p3/x)+10×exp(12.75×p2/x+12×p3/x)+12×exp(23.75×p2/x+12×p3/x)+4×exp(-16.25×p2/x+20×p3/x)+6×exp(-11.25×p2/x+20×p3/x)+8×exp(-4.25×p2/x+20×p3/x)+10×exp(4.75×p2/x+20×p3/x)+12×exp(15.75×p2/x+20×p3/x)+14×exp(28.75×p2/x+20×p3/x)+6×exp(-21.25×p2/x+30×p3/x)+8×exp(-14.25×p2/x+30×p3/x)+10×exp(-5.25×p2/x+30×p3/x)+12×exp(5.75×p2/x+30×p3/x)+14×exp(18.75×p2/x+30×p3/x)+15×exp(33.75×p2/x+30×p3/x)]+p4x (1)

p1---*g*; p2---J/k_B p3---J'/k_B p4---χ_{TIP} x---*T*

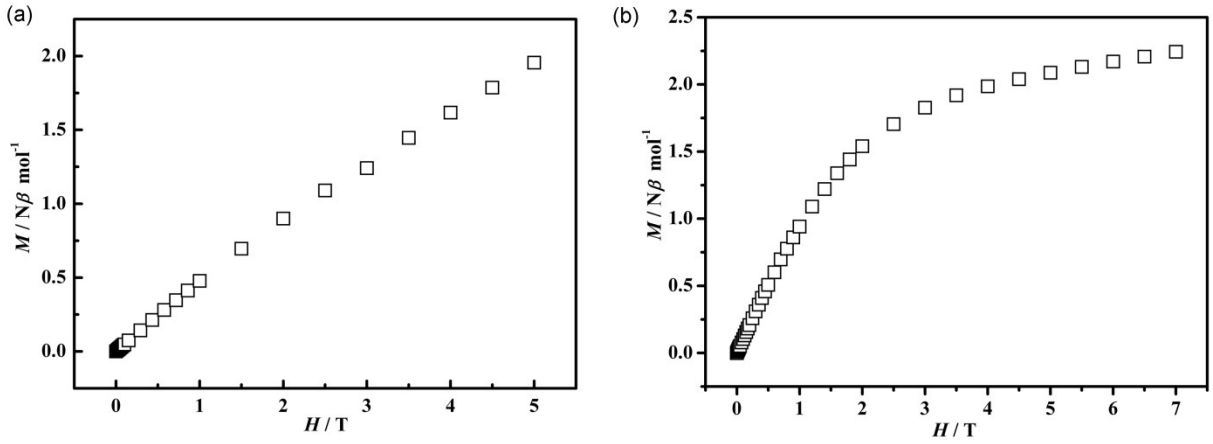

Fig. S15 The field dependence of magnetization curves for **Mn-Ac** (**a**) and **Co-DMA** (**b**) at 2 K.

References

(1) (a) G. M. Sheldrick. SHELXL-97, Program for Crystal Structure Refinement, University of Göttingen, Göttingen (Germany), **1997**; (b) G. M. Sheldrick, SHELXS-97, Program for Crystal Structure Solution, University of Göttingen, Göttingen (Germany), **1997**; (c) G. M. Sheldrick. *Acta Crystallogr., Sect. A: Found. Crystallogr*. **2008**, *64*, 112−122.